JOURNAL OF PROPULSION AND POWER
Vol. 21, No. 4, July–August 2005

Sooting of Propylene-Hydrogen Mixture Diffusion Flames with Diluents Near Smoke Point

S. F. Goh* and S. R. Gollahalli†
University of Oklahoma, Norman, Oklahoma 73019

Diluents such as steam and inert gases are used to suppress soot formation in hydrocarbon diffusion flames. The curve of the variation of the flow rate of diluent required to eliminate smoke emission from these flames with the fuel flow rate exhibits a skewed bell shape with two distinct regions. In the first region, the diluent flow rate increases with the fuel flow rate, and in the second region the trend is reversed. In a previous study these two regions were deemed to be controlled by chemical kinetics and jet momentum respectively. This study was performed to understand the dominant factors that control soot concentration in different parts of the flame in these two regions. Propylene was used as the fuel because of its high sooting tendency. The flames were always attached to the burner to avoid the complexities caused by flame liftoff. Oxygen concentration was measured by direct in-flame gas sampling. Soot and hydroxyl radical concentrations were measured using laser-induced-incandescence and laser-induced-fluorescence techniques, respectively. Results show that hydroxyl radicals play a stronger role than oxygen in both near-burner and far-burner regions of the flame in chemical-controlled region. The influence of hydroxyl radicals is significant in the near-burner region of the flame in momentum controlled region; however, the effect of oxygen is dominant in the far-burner region.

Introduction

AN extensive amount of research data exists in the literature on the smoke point of laminar flames; however, data on the smoke point in the turbulent region are scarce. Smoke point is usually defined as the condition when soot just begins to escape unburned from a laminar flame. Roper et al.[1] consider that condition as that at which the soot oxidation becomes negligibly small. Glassman and Yaccarino[2] define the smoke point as the condition where the "wings" (caused by soot breakthrough) reach the same height as the corresponding flame apex. Although there are different methods available to determine the smoke point of laminar diffusion flames,[3–5] such as determining the flame height at the condition when free smoke is liberated, no straightforward method is available to determine the smoke point of turbulent diffusion flames. Because of a lack of proportionality between the flame height and the fuel flow rate in turbulent flames, the smoke point length is not an appropriate indicator of smoking tendency of the fuel. In previous studies Goh and associates[6,7] developed a laser-based optical method to study the smoke-point characteristics of hydrocarbon diffusion flames. They also established the relation of the mass flow rate of fuels (methane, propane, and propylene) and the mass flow rate of a diluent (nitrogen) at the smoke point in both quiescent and crossflow conditions. Two distinct regions were discovered on the plot of mass flow rate of diluent required to avoid smoking with fuel flow rate. Based on the flame structure data including temperature and stable species concentrations, these regions were argued to be controlled by chemical kinetics and jet momentum.

The current study was performed to further understand the behavior of the chemical kinetics and momentum-controlled regions and to determine the dominant factors that distinguish these two regions. The flame structure was further examined with more reliable nonintrusive techniques, and transient species concentrations were measured. The relative importance of two soot oxidation pathways (O_2 and OH dominance) was investigated.

Received 18 April 2004; revision received 11 August 2004; accepted for publication 20 October 2004.

*Research Assistant, School of Aerospace and Mechanical Engineering. Member AIAA.

†Lesch Centennial Chair, School of Aerospace and Mechanical Engineering. Associate Fellow AIAA.

Experimental Techniques

Experiments were performed in a steel combustion chamber (76 × 76 cm and 143 cm high). A stainless-steel 3.2-mm ID sharp-edged tube burner was used. A 5-mW He-Ne laser beam (wavelength 633 nm) of 3 mm diam was passed through the region about 5 cm above the tip of the flame normal to its axis. When the flame started to smoke, the laser beam became visible as a result of the scattered radiation, and the intensity of the illumination of the laser beam was a function of the concentration of smoke. A viewing angle of about 15 deg from the laser beam from the forward scatter direction was found to yield repeatable and sensitive results. The fuel flow rate at the smoke point condition was determined when the laser beam just became visible continuously along its length. The details are given in Refs. 6 and 7. Flames were attached to the burner at all conditions by mixing the fuel with a small amount of hydrogen at a constant proportion. The critical fuel mass flow rate (CFMFR), defined as the maximum fuel flow rate at which the turbulent flame ceases to smoke (smoke point), was first determined. Below this fuel flow rate, the air entrainment and fuel-air mixing rate are not enough to avoid smoke emission. The fuel flow rate was then set at 10 different values: 90, 80, 70, 60, 50, 40, 30, 20, 10, and 5% of the CFMFR. At each of these flow rates, a certain amount of inert gas (nitrogen) was added to the fuel stream to achieve the smoke point condition. The nominal values of experimental parameters and uncertainties in measurements are presented in Tables 1 and 2, respectively.

Temperature, Oxygen Concentration, and Flame Height Measurement

A type R (platinum/13% rhodium platinum) in-house-made thermocouple with wire diameter of 0.2 mm and bead diameter of 0.25 mm was used to obtain temperature measurements in the flame. The bead was coated with silica to reduce catalytic reactions. The thermocouple was mounted on a linear traversing mechanism that was driven by a stepper motor. The acquisition of temperature data and the motion of the stepper motor were controlled by a computer. Temperature profiles were taken radially at three axial locations, 25, 50, and 75% of the flame height. The thermocouple data were corrected for radiative and conductive losses.[8] A gas sample was collected by using an expansion-cooled quartz probe (0.5-mm orifice diameter), and oxygen concentration in the sample was measured with a polarographic oxygen sensor. The digital flame images

Table 1 Nominal condition and experimental parameters

Parameter	Value
Fuel (vol. composition)	
Propylene	76%
Propane	20.5%
Methane	1.68%
Ethane	1.63%
Butane	0.23%
Hydrogen (purity)	99+%
Hydrogen mass fraction	0.03
Diluent nitrogen (purity)	99+%
Ambient air conditions	
Humidity	50%
Temperature	292 K
Pressure	100.6 kPa
Experimental Conditions	
Burner i.d.	3.2 mm
Fuel mass flow rate	1.03–28.87 10^{-5}kg/s
Jet velocity	6.92–38.15 m/s
Jet Reynolds number	1265–12589

Table 2 Experimental uncertainties[a]

Quantity	Uncertainty
CFMFR	0.06 μg/min
N_2 mass flow rate	0.02 μg/min
OH concentration	2.43×10^{-6} mole/m^3
Soot concentration	0.02 ppm
O_2 concentration	0.06%
Flame height	0.57 cm

[a]At 95% confidence level.

were taken during experiments, and the flame height was determined offline using an imaging software. The flame height is defined as the vertical length from the burner tip to the location of the end of the contiguous flame.

Soot Concentration Measurement

The local soot concentration was measured by using laser-induced-incandescence (LII) method. The LII employs the mechanism of heating soot particles to a temperature above the surrounding gas temperature as a result of the absorption of laser energy and the subsequent detection of the radiation (incandescence) corresponding to the elevated soot particle temperature. LII signal has a linear relationship with soot concentration at a low value of laser fluence. The laser fluence for the LII measurement was 0.34 J/cm^2. The schematic diagram of the experimental setup is shown in Fig. 1. The Gaussian profiled 1064-nm laser with pulse width of 8 ns was generated by a Nd:YAG laser operating under Q-switch condition. The detection setup was arranged perpendicular to the laser beam path. A high power-focusing lens was used to focus the beam to a size close to 1 mm diam at full-width half-maximum. The laser induced incandescence (LII) signal from C_2 swan band extends from $\approx$420 to 620 nm, and it peaks at 516.5 nm. A short-pass dielectric (central wavelength of 437 nm and bandwidth of 9 nm at half the maximum transmission) filter was used for this study. Although it is in the C_2 swan band, the interference is small because it is at the minimum starting edge of the band. Most of the literature used a detection wavelength around 400 to 450 nm. An intensified change coupled devise (ICCD) camera with an array size of 576×384 pixel synchronized with the laser pulse was used to capture the image. Image data were sent to a PC-based image-acquisition system. The LII signal was calibrated by duplicating the experiments of Shaddix and Smyth.[9] We reconstructed the burner they had used (1.1 cm i.d., 10.2 cm i.d. annulus) and repeated their experiments with propane (flow rate 2.57 cm^3/s) and coflow air (flow rate 694 cm^3/s).

Hydroxyl Radical Concentration Measurement

The laser-induced-fluorescence (LIF) experimental setup was somewhat similar to the LII setup. The laser equipment used for LIF measurements consisted of a pulsed Nd:YAG laser coupled

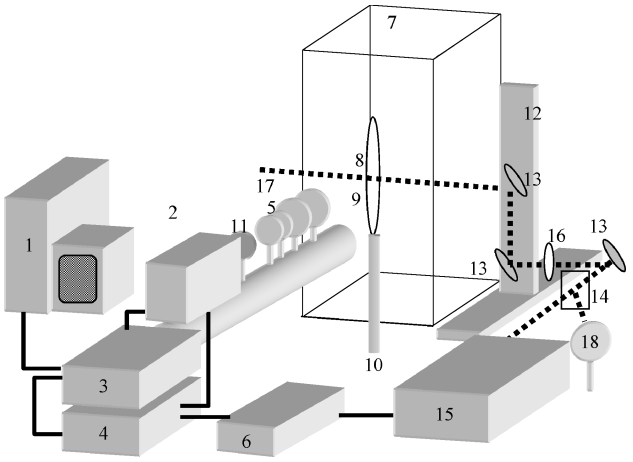

Fig. 1 Schematic of experimental setup: 1, computer with DAQ; 2, ICCD camera; 3, camera controller; 4, camera gate and trigger; 5, optical lenses; 6, pulse generator; 7, combustion chamber; 8, flame; 9, burner; 10, to fuel supply train; 11, 431-nm filter; 12, X-Y traverse mechanism; 13, 1064-nm mirror; 14, beam splitter; 15, Nd:YAG laser; 16, focusing lenses; and 17, 1064-nm laser beam.

to an optical parametric oscillator with a frequency doubler option (FDO). The same ICCD camera system with a different bandpass filter was used for detection of OH. For OH measurement, a frequency-doubled output (285.26 nm) of the FDO was used to induce fluorescence,[10] which was detected at a wavelength of 315 nm. At this wavelength, OH was pumped at the $Q_1(6)$ transition in the OH $A^2 \sum \leftarrow X^2 \prod$ system of the (1,0) band and the fluorescence from the (1,1) band was collected.[11] A narrowband pass filter (central wavelength of 314.59 nm and bandwidth of 10 nm at 50% of maximum transmission) was used. To isolate the interference signal of LII and other species, a second set of data was obtained with an off-resonance frequency (285.285 nm) laser. The OH signal was the result of the subtraction of the signal at the resonance frequency and the signal at the off-resonance frequency. With this method, LIF results were isolated from LII signal and interference from other species. For both LII and LIF measurements, an excitation beam of diameter of 1 mm was used. For a diffusion flame in atmospheric condition, only 3 out of 1000 excited OH radicals lose energy through fluorescence, and the rest of the molecules lose their energy through collisional quenching with ambient gases.[12] For the quantification of OH radical concentration, a commonly used method is the direct estimation of the quenching rate at the location of the measurement to determine the quantum yield. This method requires the concentration field of species involved and is relatively less complicated and more feasible. The concentration and the local flame temperature can be obtained from the numerical results. The details of spectroscopic modeling are given by Laufer,[13] and was adopted in this study. The collision species that were used for the calculation were N_2, O_2, CO, CO_2, H_2, H_2O, CH_4, H, and OH whose concentrations were obtained from the computational results using an equilibrium model. Because the numerical model predictions agreed well with the measured results for the major species (O_2 and CO_2) concentrations and flame temperature, they were considered reasonable for quenching rate calculation. Because the goal of our project was to understand the dominant processes on the two sides of the transition region in the diluent flow rate-fuel flow rate curve at the smoke point, this procedure is considered reasonable. Collisional quenching parameters of Tamura et al.[12] were used.

Results and Discussion

Figure 2 shows a plot of diluent mass flow rate with fuel mass flow rate at smoke point. The critical fuel mass flow rate of fuel without the diluent addition (CFMFR) was 0.017 kg/min. At this condition the exit jet velocity and Reynolds number were 38.15 m/s and 12.589×10^3, respectively. The decrease of fuel mass flow rate from CFMFR required an increase of diluent amount to reattain the smoke-point condition (considered momentum-controlled

region[6,7]). At approximately 30% CFMFR (fuel flow rate at 0.005 kg/min), there was a transition. Below this point, the diluent mass flow rate decreased with the continued decrease of fuel mass flow rate (considered as chemically controlled region[6,7]). We initially hypothesized that transition from turbulent to laminar condition could be the reason for the difference between the two regions; however, the flame photographs, visual observations, and instantaneous temperature data did not support our hypotheses. Only for very low flow rates (approximately 5% CFMFR) the flames appeared laminar. One fuel/diluent flow rate condition from each region was selected for the diagnostic study presented here. A flame at 10% CFMFR was selected to represent the chemically controlled region, and the 60% CFMFR flame was selected to typify the momentum-controlled region.

To investigate the reasons for the distinction of these regions, the in-flame OH and soot concentrations were measured. The radial concentration profiles of OH and soot at a distance of 25 and 50% of the flame height (H) above the burner for 10% (chemically controlled) and 60% (momentum-controlled) CFMFR were measured. The flame images at smoke-point conditions at different values of CFMFR are shown in Fig. 3. The concentration results are plotted in Figs. 4–9.

At 25 and 50% of flame height of the 10% CFMFR flame (Figs. 4 and 5), both soot and OH concentration profiles exhibit off-axis peaks. The soot concentration peak is on the inside of the OH peak, which agrees with many OH-soot concentration results for a laminar flame.[14,15] The OH and soot overlapping region is where the active soot oxidation occurs.[15] In the 10% CFMFR flame, the soot particles in the flame have to rely on OH for oxidation as a result of a lower degree of air entrainment caused by the lower jet velocity, that is, OH radical dominates the soot oxidation in this region. This result agrees with laminar flame studies by Neoh et al.[16] and Garo et al.[17] For a laminar diffusion flame, the OH continues to dominate the soot oxidation process until the O_2 concentration is sufficiently high. Oxygen is intrinsically less reactive than OH radical, so that the O_2 molecule is able to penetrate deeper only into the open spaces within the soot aggregates towards the end of the flame. The OH radical participates actively in the surface oxidation of soot over most of the flame height. The combination of the internal oxidation of the soot particles (by O_2) and the surface regression caused by the external oxidation (by OH) could also lead to the breakup of the soot particles. The breakup is supposed to occur only after 80% of the initial mass has been oxidized.[16,17] The argument about the dominance of OH on soot oxidation is also supported by the oxygen concentration profiles. Figure 8 shows that at 25, 50, and 75% of the flame height the O_2 concentration at the center of the flame was 2.5, 5.5, and 11%, respectively. According to Neoh et al.,[16] OH dominates the soot oxidation process in a region with O_2 concentration between

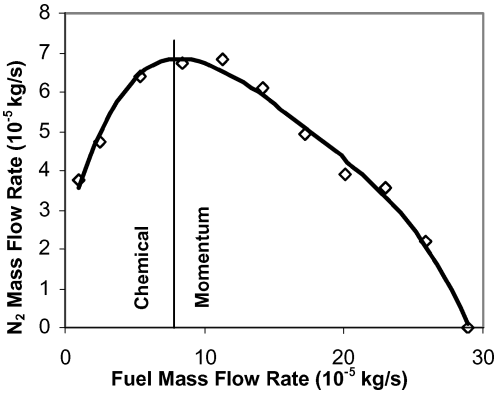

Fig. 2 Chemical and momentum dominated regions in a propylene diffusion flame with smoke suppression by nitrogen addition to the fuel stream.

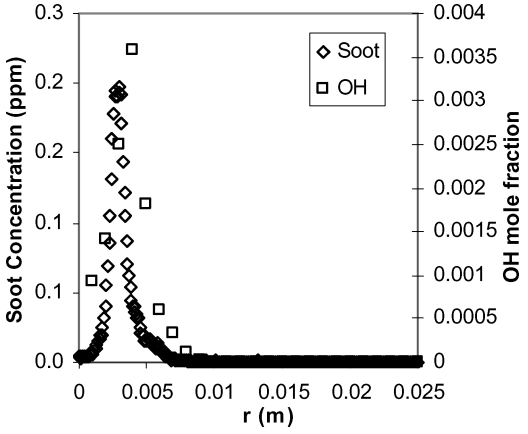

Fig. 4 Radial profiles of soot and hydroxyl radical concentration at 25% flame height in the 10% CFMFR flame.

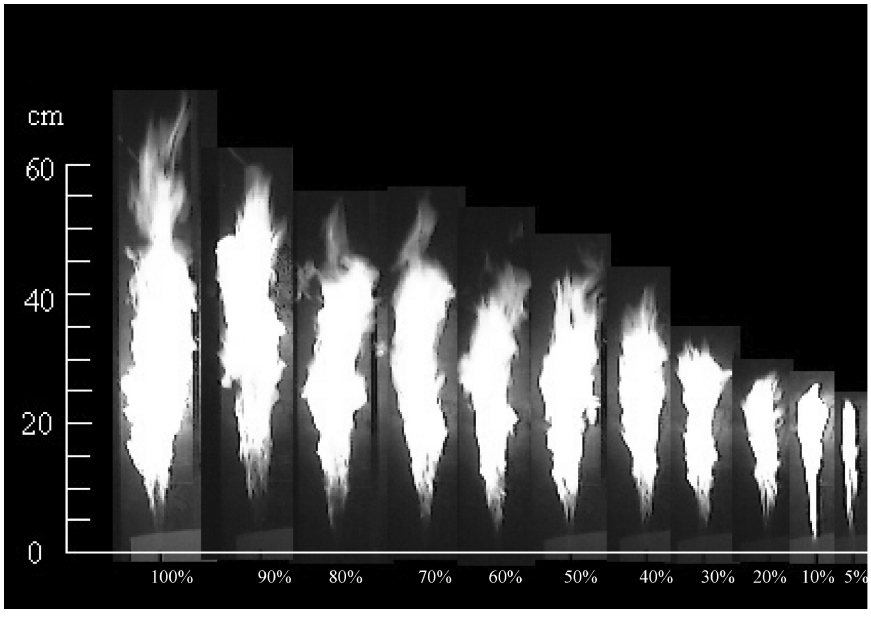

Fig. 3 Images of nitrogen-diluted propylene diffusion flames with different fuel flow rates (%CFMFR) at smoke point.

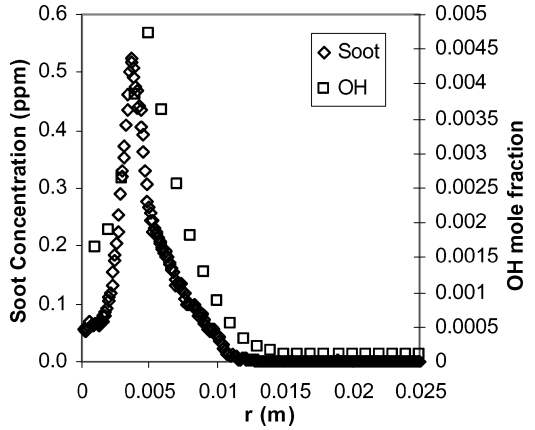

Fig. 5 Radial profiles of soot and hydroxyl radical concentration at 50% flame height in the 10% CFMFR flame.

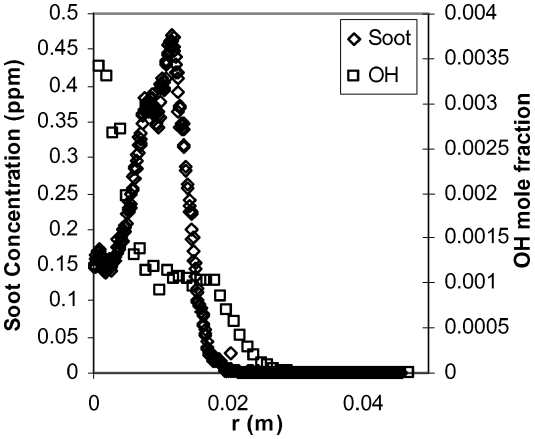

Fig. 6 Radial profiles of soot and hydroxyl radical concentration at 25% flame height in the 60% CFMFR flame.

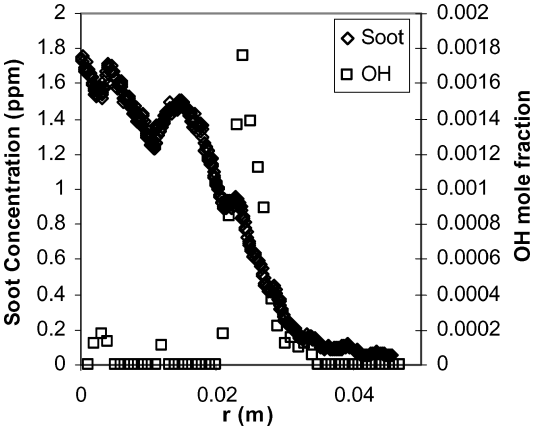

Fig. 7 Radial profiles of soot and hydroxyl radical concentration at 50% flame height in the 60% CFMFR flame.

0.001 and 5%. In the region, from 50% to 75% of the flame height the dominance of the soot oxidation process seems to shift from OH to O_2. Thus, the OH radical dominates most part soot oxidation process in the 10% CFMFR flame at the smoke point.

At 25% flame height of the 60% CFMFR flame (Fig. 6), the OH radial concentration profile does not show an off-axis peak. OH concentration drops rapidly until midway between the flame axis and the edge and levels off until the flame edge before falling off to zero. The soot concentration profile, on the other hand, exhibits an off-axis peak located closer to but inside of the flame edge. At

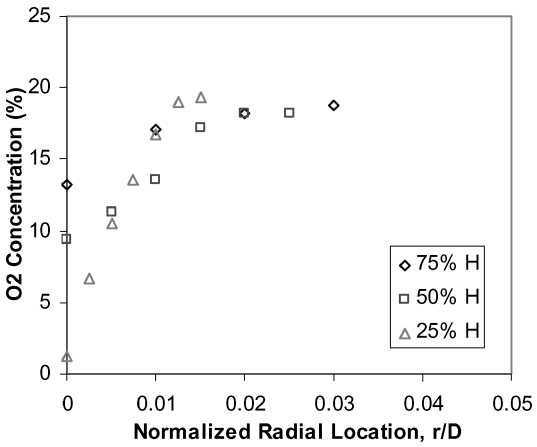

Fig. 8 Radial oxygen concentration profiles in the near-burner (25%H), midflame (50%H), and far-burner (75%H) regions in the 10% CFMFR flame.

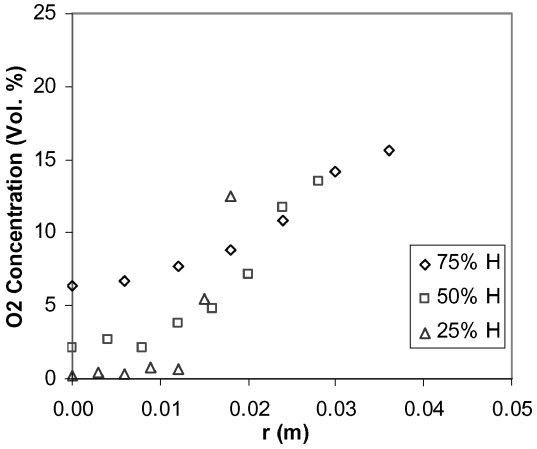

Fig. 9 Radial oxygen concentration profiles in the near-burner (25%H), midflame (50%H), and far-burner (75%H) regions in the 60% CFMFR flame.

50% flame height of the 60% CFMFR flame (Fig. 7), however, the soot and OH concentration peaks do not occur at the same relative location. OH concentration peaks on an off-axis location closer to the flame edge, whereas soot concentration profile peaks on the flame axis. Soot concentration is low where OH peak occurs, and OH concentration is negligible where much of soot is present. The lack of this overlapping region means that the OH radical does not play a dominant role in the oxidation of soot at this flame location. Certainly, the role of OH is not as significant as at the 25% flame height of the 60% CFMR and 10% CFMFR flames. Hence, at this region O_2 dominates the oxidation of soot particles rather than OH radical. The 60% CFMFR turbulent flame entrains larger amounts of O_2 from the surrounding air than the 10% CFMFR laminar flame, and thus soot oxidation by O_2 becomes more significant (Fig. 9).

According to Kent and Wagner,[3] the difference between a laminar flame and a turbulent flame at the region close to the burner is that the soot generation or oxidation is kinetically controlled in a laminar flame, but it is diffusion controlled in a turbulent flame. In the far-burner region, where soot concentration is high, the heat release in laminar flames are controlled by the local concentration of oxygen containing species.[3] In this study, however, the oxygen-containing species responsible for soot burnout in most of the 10% CFMFR flame was OH radical, and in the 60% CFMFR flame was O_2 molecule. The 60% CFMFR flame had a lower flame temperature at 50% flame height (Fig. 10) and higher CO concentration.[18] Higher CO concentration reduces the availability of OH radical to react with soot particle, which provides another factor supporting the importance of O_2 molecule in soot oxidation.

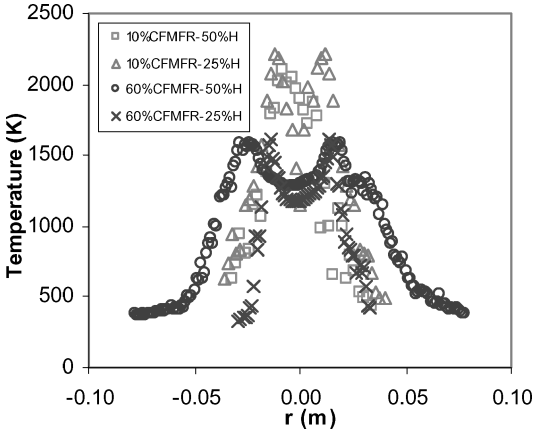

Fig. 10 Radial temperature profiles in the 10 and 60% CFMFR flames at 25 and 50% flame height (H).

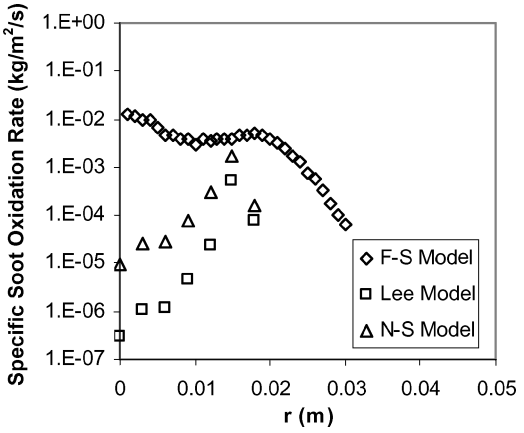

Fig. 11 Comparison of specific soot oxidation rate by hydroxyl radical and oxygen in the 60% CFMFR flame calculated with Fenimore and Jones (F-J), Nagle and Strickland-Constable (N-S), and Lee et al. (Lee) models at 25% flame height.

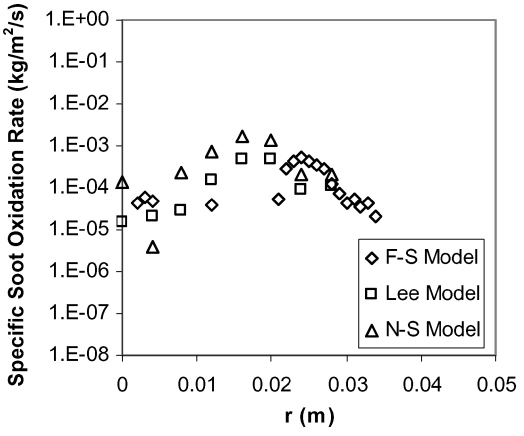

Fig. 12 Comparison of specific soot oxidation rate by hydroxyl radical and oxygen in the 60% CFMFR flame calculated with Fenimore and Jones (F-J), Nagle and Strickland-Constable (N-S), and Lee et al. (Lee) models at 50% flame height.

To further substantiate this result, the specific soot oxidation rates with OH and O_2 were calculated based on Lee et al.[19] and Fenimore and Jones.[20] Lee et al. assumed spherical particles with uniform initial diameter, and the reaction occurred on the external surface. Fenimore and Jones also assumed uniform spherical particles reacting at a constant rate per unit surface area. In these calculations, α is the collision efficiency for OH, which is not a constant value but ranges from 0.01 to 0.11 (Ref. 21). Because this value was not known priory, $\alpha = 0.1$ was assumed following Ref. 19. Also, the local partial pressures of OH and O_2 (P_{OH} and P_{O_2}), and the local flame temperature T were taken as the experimental measurements in Goh.[18] At 25% flame height of the 60% CFMFR flame (Fig. 11), OH contribution is higher than that of O_2 on the flame axis and most of the core region. At the flame edge, the contribution of O_2 peaks as a result of the higher availability of O_2 (Fig. 9). Furthermore, Fig. 12 shows that in the same flame at 50% flame height O_2 role far surpasses that of OH.

From these observations, we conclude that soot oxidation by OH was more significant in the 10% CFMR flame than in the 60% CFMR flame in Fig. 2. Because the local OH concentration is chemical reaction rate controlled[22] and O_2 concentration is diffusion controlled, the dominance of either OH or O_2 validates the dominance of chemically controlled and momentum-controlled mechanisms for the regions left and right of the peak in Fig. 2.

Conclusions

The experimental results include the radial concentration profiles of soot, oxygen, and hydroxyl radical in two typical flames (at 10 and 60% of the critical fuel mass flow rate, CFMFR) of nitrogen diluted propylene-hydrogen mixture diffusion flames at smoke point. These flames represent two differently varying regions on the diluent flow rate vs fuel flow rate curve at the smoke point. The current results have been analyzed in conjunction with earlier documented stable species and temperature measurements to determine the dominant mechanisms responsible for the distinct behavior in these two regions. Hydroxyl radical plays a stronger role than oxygen in both near-burner and far-burner regions of the 10% CFMFR flame (in chemical controlled region). Although the influence of hydroxyl radical is significant in the near-burner region of the 60% CFMFR flame (in momentum-controlled region), the effect of oxygen is dominant in the far-burner region.

References

[1]Roper, F. G., Smith, C., and Cunningham, A. C., "The Prediction of Laminar Jet Diffusion Flame Sizes: Part II Experimental Verification," *Combustion and Flame*, Vol. 29, No. 3, 1977, pp. 227–234.

[2]Glassman, I., and Yaccarino, P., "The Effect of Oxygen Concentration on Sooting Diffusion Flames," *Combustion Science and Technology*, Vol. 24, Nos. 3–4, 1980, pp. 107–114.

[3]Kent, J. H., and Wagner, H. G., "Why Do Diffusion Flames Emit Smoke?" *Combustion Science and Technology*, Vol. 41, Nos. 5–6, 1984, pp. 245–269.

[4]Roper, F. G., "Soot Escape from Diffusion Flames: A Comparison of Recent Work in This Field," *Combustion Science and Technology*, Vol. 40, 1984, pp. 323–329.

[5]Glassman, I., and Yaccarino, P., "The Temperature Effect in Sooting Diffusion Flames," The Combustion Inst., Pittsburgh, PA, 1981, pp. 1175–1183.

[6]Goh, S. F., Kusadomi, S., and Gollahalli, S. R., "Effects of Burner Diameter and Fuel Type on Smoke Point and Radiation Characteristics of Diffusion Flames," *Engineering Technology Conference and Exhibition*, Houston, TX, 4–6 Feb. 2002; also Paper ETCE/CAE-29011, American Society of Mechanical Engineers, New York, 2002.

[7]Goh, S. F., "Experimental Studies of Diffusion Flame Smoke Point in Quiescent and Cross-Flow Environments," M.S. Thesis, School of Aerospace and Mechanical Engineering, Univ. of Oklahoma, Norman, Aug. 1999.

[8]Fristrom, R. M., and Westenberg, A. A., *Flame Structure*, McGraw–Hill, New York, 1965.

[9]Shaddix, C. R., and Smyth, K. C., "Laser-Induced Incandescence Measurement of Soot Production in Steady and Flickering Methane, Propane, and Ethylene Diffusion Flames," *Combustion and Flame*, Vol. 107, No. 4, 1996, pp. 418–452.

[10]Battles, B. E., Seitzman, J. M., and Hanson, R. K., "Quantitative Planar Laser Induced Fluorescence Imaging of Radical Species in High Pressure Flames," AIAA Paper 94-0229, Jan. 1994.

[11]Hanson, R. K., "Combustion Diagnostics: Planer Image Techniques," *Proceedings of the Twenty-First Symposium (International) on Combustion*, The Combustion Inst., Pittsburgh, PA, 1986, pp. 1677–1691.

[12]Tamura, M., Berg, P. A., Harrington, J. E., Luque, J., Jeffries, J. B., Smith, G. P., and Crosley, D. R., "Collisional Quenching of CH(A), OH(A), and NO(A) in Low Pressure Hydrocarbon Flames," *Combustion and Flame*, Vol. 114, Nos. 3–4, 1998, pp. 502–514.

[13]Laufer, G., *Introduction to Optics and Lasers in Engineering*, Cambridge Univ. Press, New York, 1996.

[14]Puri, R., Moser, M., Santoro, R. J., and Smyth, K. C., "Laser-Induced Fluorescence Measurement of OH Concentrations in the Oxidation Region of Laminar, Hydrocarbon Diffusion Flames," *Proceedings of the Twenty-Fourth Symposium (International) on Combustion*, The Combustion Inst., Pittsburgh, PA, 1992, pp. 1015–1022.

[15]Smyth, K. C., Shaddix, C. R., and Everest, D. A., "Aspects of Soot Dynamics as Revealed by Measurements of Broadband Florescence and Flame Luminosity in Flickering Diffusion Flames," *Combustion and Flame*, Vol. 111, No. 3, 1997, pp. 185–207.

[16]Neoh, K. G., Howard, J. B., and Sarofim, A. F., "Effect of Oxidation on the Physical Structure of Soot," *Proceedings of the Twentieth Symposium (International) on Combustion*, The Combustion Inst., Pittsburgh, PA, 1984, pp. 951–957.

[17]Garo, A., Prado, G., and Lahaye, J., "Chemical Aspect of Soot Particle Oxidation in a Laminar Methane-Air Diffusion Flame," *Combustion and Flames*, Vol. 79, Nos. 3–4, 1990, pp. 226–233.

[18]Goh, S. F., "An Experimental and Numerical Study of Diffusion flame in Cross-Flow and Quiescent Environment at Smoke Point Condition," Ph.D. Dissertation, School of Aerospace and Mechanical Engineering, Univ. of Oklahoma, Norman, July 2003.

[19]Lee, K. B., Thring, M. W., and Beer, J. M., "On Rate of Combustion of Soot in Laminar Soot Flame," *Combustion and Flame*, Vol. 6, No. 3, 1962, pp. 137–145.

[20]Fenimore, C. P., and Jones, G. W., "Oxidation of Soot by Hydroxyl Radicals," *Journal of Physical Chemistry*, Vol. 71, No. 3, 1967, pp. 593–597.

[21]Haudiquert, M., Cessou, A., Stepowski, D., and Coppalle, A., "OH and Soot Concentration Measurements in a High-Temperature Laminar Diffusion Flame," *Combustion and Flame*, Vol. 111, No. 4, 1997, pp. 338–349.

[22]Puri, R., Santoro, J., and Smyth, K. C., "Oxidation of Soot and Carbon Monoxide in Hydrocarbon Diffusion Flames," *Combustion and Flame*, Vol. 97, No. 2, 1994, pp. 125–144.